A eukaryote assemblage intercalated with Marinoan glacial deposits in South Australia

D.P. LE HERON, D.H.M. ALDERTON, M.E. COLLINSON, N. GRASSINEAU, A.E. TRUNDLEY.

Royal Holloway University of London, Egham, Surrey, UK, TW20 0EX, UK.

Abstract: Composite hematite-silica structures recovered from a siltstone bed in the Elatina Formation of South Australia include (1) sub-circular to whorl-shaped forms, (2) elongate to half-moon shaped and (3) and lozenge-shaped forms locally linked into chains. They range 200-500 µm in diameter and are interpreted as eukaryote tests. Evidence for internal etching of a calcite core of some tests indicates that at least some of the hematite-silica fabrics were acquired through replacement. Carbon isotope values of -20‰ $\delta^{13}C$ are suggestive of precipitation by microbial activity, and imply a change in ambient fluid chemistry associated with a pH reduction. The tests occur within sandstone beds that were deposited on a tidally-modulated braidplain during the Marinoan glaciation at the end of the Cryogenian. The quartz grains in the sandstone sample lack the typical textures (surface striae, internal fractures, or irregular grain boundaries) expected for glacially-transported material. Thus, on textural grounds we argue that the eukaryote tests represent a proglacial ecosystem during a late Cryogenian snowball Earth event.

The relationship between Neoproterozoic glaciation and the evolution of eukaryotes has been a major topic in Precambrian research for more than three decades (Vidal and Knoll, 1982; Knoll et al., 2006; Kirschvink, 1992; Hoffman et al., 1998; Fairchild and Kennedy, 2007; Le Heron, 2012). Cryogenian (720-635 Ma) strata, deposited during a global interval of intense glaciation, contain a sparse but important archive of fossil eukaryotes. These include possible fragments of ancestral sponges in the central Flinders Ranges of Australia (Maloof et al., 2010), sponge-like chambered fossils (central Namibia: Brain et al., 2012), putative foraminiferal tests (northern Namibia: Bosak et al., 2012), and agglutinated eukaryote tests also in northern Namibia (Dalton

et al., 2013). The last examples come from a succession forming part of a post-glacial cap carbonate sequence (Hoffman and Halverson, 2008).

In spite of these discoveries, “the glacial interval is mostly shrouded in mystery”, because most fossil finds come from the so-called Late Cryogenian Warm Interval (LCWI) below the Marinoan glacial succession (Shields-Zhou et al., 2012). Even in that interval, the biological affinity of many “fossils” remains contentious, or at least difficult to interpret. Centimetre-scale discoid structures from Kazakhstan, found beneath a glacial diamictitite, are a prime example where Meert et al. (2011) openly acknowledge that depending on one’s stance, “a bacterial, lichen, Vendobiont, or non-biogenic interpretation” is possible for discoidal impressions on bedding planes beneath an undated diamictite. Well-preserved assemblages of leiosphaerid acritarchs were described in both glacial (Sturtian) and LCWI by Riedman et al. (2014). The problems of interpretation for body fossils were reviewed, specifically for microbe-like forms, by Schopf et al. (2010) who recommended multi-disciplinary approaches. In this paper, we report the occurrence of unusual sand-sized, ferruginous agglutinates interpreted as eukaryote fossils in glacially-related strata of the Elatina Formation, South Australia. This is very important because although fossil material is common to many glacially-related successions (e.g. stromatolites in the Marinoan of Svalbard: Fairchild et al., in press), there have thus far been no reports of eukaryotes *sandwiched between* glaciogenic diamictite beds in the Marinoan record.

Here, we present fossil material from South Australia, extracted from the Elatina Formation which was deposited in a topographically subdued, glacial outwash plain (Williams et al., 2008). This formation represents the Marinoan glaciation in the

Flinders Ranges (Rose et al., 2013). Well preserved whorl-shaped fossils and linked lozenges, composed largely of hematite, are tentatively interpreted as an assemblage of eukaryote tests partially replaced as a result of bacterial activity. This highly unusual assemblage, and its context in glaciogenic strata, sheds new light on a Cryogenian proglacial ecosystem, and the survival of life during intense snowball Earth glaciations (see Le Heron, 2012 for a review).

Setting, Stratigraphy and Sedimentology

Neoproterozoic strata of the Flinders Ranges (**Fig. 1**) expose classic Cryogenian glacial successions separated by interglacial strata: a lower, Sturtian interval and an upper, Marinoan record (Mawson, 1949a, b; Mawson and Sprigg, 1950). The interglacial succession is now recognised to belong to the LCWI (Shields-Zhou et al., 2012). Post-Sturtian black shales, recording the base of the LCWI succession, yield a date of ~ 643±2.4 Ma (Re-Os: Kendall et al., 2006); some several hundred metres upsection, a date of 659.7±5.3 Ma (authigenic monazite) was published by Mahan et al., 2010). Whilst incongruent, these results place a maximum age constraint on the fossils described in this paper. A minimum age constraint is provided by the Cryogenian-Ediacaran GSSP, 1000 m from our study area, (635 Ma: Knoll et al., 2004). Palaeomagnetic data collected from the Elatina Formation demonstrates Australia's tropical location during the Marinoan glaciation: Schmidt and Williams (1995) obtained a value of 2.7°±3.7° N, whereas Sohl et al. (1999) obtained a palaeolatitude of 7.5° N based on "very reliable" palaeomagnetic data that passed fold tests at the 99% significance level. The putative demosponges were recovered by Maloof et al. (2010) from the Trezona Formation, (**Fig. 2**), a few hundred metres

below the Elatina Formation in the upper levels of LCWI strata. The Elatina Formation itself remains poorly dated, although Ireland et al. (1998) published a detrital zircon age date of 649±17 Ma based on two samples.

Sedimentology of the Elatina Formation

In general terms, the Elatina Formation represents the deposits of a glacially-influenced continental setting with a marginal marine influence (Williams et al., 2008; Rose et al. 2013). In the central Flinders Ranges, a sandstone-dominated succession is punctuated by diamictite at intervals. The sandstones are interpreted as fluvial sandur deposits (Williams et al., 2011; Rose et al., 2013); to the west of the Flinders Ranges, the succession cropping out on the Stuart Shelf yields aeolianites (Ewing et al., 2014). The absence of deep fjordal topography, and the lateral continuity of facies associations (Le Heron et al., 2011), collectively suggests deposition on a topographically subdued continental shelf area.

At Brachina Gorge, 22.5 m of the Elatina Formation is exposed (**Fig. 3**); this is overlain by the Nuccaleena cap dolostone which also marks the Ediacaran Global boundary Stratotype Section and Point (GSSP: Knoll et al., 2004; Preiss, 2005; Raub et al., 2007; Rose and Maloof, 2010). At Brachina Gorge, four lithofacies are recognised: (i) heterolithic intervals with sandstone and mudstone interbeds, (ii) cross-stratified sandstones (iii) muddy diamictites, and (iv) shale and siltstone, some beds of which contain lonestones.

The heterolithic intervals record intercalation of sandstone and shale laminae on a centimetric scale. Evidence of cm-scale deformation beneath sandstone layers,

including flame structures, together with intrabed folds in sandstone layers themselves, is commonplace (**Fig. 3; Fig. 4 A, A'**). Delicately preserved cross-laminations are recognised, and thickness variations on some lamina foresets, together with clay drapes on others, are noted (**Fig. 3; Fig. 4 A, A'**). Scour and fill geometries occur both within the heterolithic facies (**Fig. 3; Fig. 4 A, A'**) and also in more continuous intervals of cross stratified sandstones (**Fig. 3; Fig. 4 B, B'**). In the latter, climbing ripple geometries are well-developed, with individual sets revealing subtle reactivation surfaces and clay drapes. Two intervals of silty diamictite are exposed at Brachina Gorge (**Fig. 3**). Diamictite deposits are highly friable with very poor outcrop quality, although some diffuse stratification, some of which is deflected by lonestones, can be observed. Downlap of cross-stratified sandstone onto the upper surface of the lower diamictite are noted (**Fig. 3; Fig. 4 C, C'**). The microfossils described in this paper derive from this sandstone bed, 16 m from the base of the measured section (**Fig. 3**). Noteworthy in this bed are the presence of both symmetrical ripple forms of cross-bed foresets, and counter-current cross laminations along cross-bed foresets (**Fig. 3; Fig. 4 D, D'**).

The lithofacies described above both set the context for fossil material described in this paper and illustrate that a clear tidal influence can be demonstrated in Brachina Gorge. Multiple features strengthen this interpretation, notably (i) the cm-scale heterolithic intercalations are interpreted as flaser beds, (ii) the thickness variations of some lamina foresets are interpreted as tidle bundles, (iii) the clay-draped foresets represent slackwater deposition at the turning tide, (iv) the scour and fills record shifting loci of erosion and deposition, (v) reactivation surfaces imply reworking at the turning tide (Davis and Dalrymple, 2011). The presence of counter-

current ripples on cross-bed foresets probably represents the effects of both flood and ebb tide interaction, although it should be noted that counter-current ripples can form in various other environments, wherever separation eddies can be generated (Herbert et al., 2015). Elsewhere in the Flinders Ranges, there is strong evidence for a tidal influence in the Elatina Formation, including classical rhythmites in the Reynella Siltstone Member (Williams et al., 2008; Ericsson and Simpson, 2011) and ladderback ripples (Le Heron et al., 2011).

The poor preservation quality of the diamictite deposits stymies detailed analysis of these deposits at either the macro-or micro-scale. However, given the context above of a topographically subdued, tidally modulated braidplain, it is proposed that the diamictites are of direct glacial derivation. The topographic context implies that interpreting them as the products of downslope instability would likely be erroneous in this case. Therefore a fluctuating ice margin at or near sea level, as proposed under the snowball Earth hypothesis (Hoffman et al., 1998), is supported by the sedimentological evidence.

Analysis of fossil material

Methodology: preparation of fossil material

A single 100 g sample was collected from a siltstone interbed in tidal cross-stratified strata in Brachina Gorge (**Fig. 3**) for standard thin section analysis. For scanning electron microscope (SEM) analysis, a sub-sample was etched in 10% dilute HCl for 30 seconds, partly destroying the calcite cement but enabling the fossil material to stand in relief on the etched surface. Nano-Computerised Tomography (N-CT) analyses were undertaken to determine the 3-dimensional structure of the fossil material. A second sub-sample was shaped into a cylinder of 5 mm diameter and 40 mm length and examined using the Nano-CT scanner at the Natural History Museum, London. Elemental mapping was

undertaken on a FEI Quanta 200F field emission SEM at King's College, University of London. Bulk specimen mineralogy was assessed using an X-ray spectrometer. Stable carbon isotope analysis was undertaken as follows. Sub-samples were cleaned with methanol, de-carbonated in 20% HCl solution for 4 hours at 100˚C and rinsed three times. These were then flash-combusted at 1800˚C and analysed by continuous flow with an Elemental Analyser coupled on-line to IR-Mass Spectrometer, according to the methodology described by Grassineau (2006). Analytical precision on standards is ±0.1‰. Note that sample collection was undertaken 750 m south of the Ediacaran GSSP (Knoll et al., 2004) from a very discrete location (31°20.316'S 138°37.871'E) so as not to damage rocks at this important locality.

Description

In thin section, silt-grade grains of quartz, opaque objects and feldspar are observed (**Fig. 5**). The grains are cemented by calcite (drusy equant spar). XRD analysis reveals that quartz (36%) and calcite (49%) and alkali feldspar (8%) predominate. Chlorite (4%) and hematite 4% are also present. Quartz grains are smooth-textured, lack striations, and are sub-rounded to rounded.

Opaque objects range in diameter from 200-500 µm. These show a sharp external wall, but a continuum of sharp to diffuse texture from the inner wall to the core of the structure. In some examples, the entirety of the object is opaque, from rim to core, whereas in others, large (200-300 µm) single or multiple crystals of calcite form a core with the opaque material outlining the rim. In the latter cases, a diffuse boundary between the inner wall of the opaque objects and the calcite core is evident. Three opaque object shape groups are identified: 1), sub-circular forms, including some with a whorl geometry that are calcite-cored; 2), elongate to half-moon forms; 3), lozenge-shapes, locally organised into chains (**Fig. 5** A, C). In the chain configuration, hook-shaped terminations bind the lozenges together (**Fig. 5** A).

Scanning electron microscope (SEM) analysis (**Fig. 5** C, D) clearly reveals the whorl and lozenge shapes, together with partially etched calcite cores and cement from sample preparation. The material making up the opaque objects is characterised by its heterogeneous, spotty texture, suggesting that they are composed of multiple mineral phases (**Fig. 5** C). Nano-CT analysis (**Fig. 5** E, F) demonstrates that the whorl-shaped structures are sub-spherical, and illustrates that half-moon forms are dominant. Elemental mapping by SEM allows the distribution of Fe and Si to be assessed (**Fig 5** G-I). These data demonstrate that hematite detected from XRD analysis corresponds to the opaque objects. The concentration of Si in the opaques suggests that the heterogeneous, spotty material also includes a quartz or microcrystalline silica phase. Stable isotope data reveal a negative $\delta^{13}C$ value of -20‰ for the opaque objects (**Table 1**).

Although we were not successful in our attempts to isolate the material following partial digestion in acid, investigation of different parts of the etched slide (**Fig. 6**) permits deeper insight into the range of forms and scales for the opaque objects, together with their relationship to the host rock. For instance, **Fig. 6** A clearly demonstrates close association between the chains of lozenges and the sub-circular forms; **Fig. 6** B shows that whereas some of the opaque objects are fully composed of spotty-textured Fe and Si, in other examples the sub-circular forms are identifiable only by a thin “rind”, with a large calcite core. The whorl-shaped forms (**Fig. 5** C, **Fig. 6** C) are by far the largest opaque objects (300 µm) observed. In some cases these are conjoined with the lozenge-shaped fabrics (**Fig. 6 C**, D). The full range of 100% Fe-Si forms, to an estimated 10% Fe-Si (i.e. very large calcite cores) is shown in **Fig. 6** F-H.

Interpretation

Any interpretation for the Elatina opaques must explain their size, range of forms in the material, and iron-rich composition. It is proposed that non-biogenic interpretations are inadequate. Hematite framboids are typically much smaller (3-23 μm and as globules: Loughbreed and Manusco, 1973). The structures are not ferriferous ooids (e.g. Bhattacharyya and Kakimoto, 1982) as they lack concentric structures. A biogenic explanation must account for both external character (sub-spherical geometries and interconnected lozenges) and internal characteristics (heterogeneous or spotty material). It is proposed that the opaques are eukaryote tests that have possibly undergone later replacement. The diffuse internal boundary of some tests, and lack of sharp interior wall, indicates that the heterogeneous, spotty texture is secondary. The continuum of textures in some examples, in concert with the very irregular contact between whorl-shaped tests and calcite "cores" in others (**Fig. 5** B, C), suggests that the hematite-silica rinds were deposited by a secondary (replacement) process. This idea is supported by the sharply defined exterior wall to each of the tests.. The stable isotope data from the tests is supportive of such a biogenic replacement mechanism. The values of -20‰ $\delta^{13}C$ from the opaques are consistent with ratios expected of eukaryotic algae, cyanobacteria, anoxic photosynthetic bacteria and methanogenic bacteria (Prashnowsky, 2002). This is a clear biogenic signal, given that there is no outcrop evidence for later hydrothermal activity that might otherwise explain this value (Raub et al., 2007; Rose and Maloof, 2010).

A simple taphonomic model is presented on **Fig. 7.** This model proposes that an assemblage of calcite tests were deposited along with quartz sand, and that carbonate precipitation was possible in alkaline waters (**Fig. 7 A**). Following deposition, pore water chemistry evolved to a more acidic composition (Fig. 7 B), promoting etching of the tests and the development of a replacement hematite-silica rind. This rind developed more fully with time (**Fig. 7 C**) whereby some calcite tests were completely replaced by the hematite-silica material. Later, during diagenesis, porewaters reverted to a more alkaline trend, facilitating the precipitation of calcite rhombs as equant spar cements within all available pore space (**Fig. 7 D**).

Given the $\delta^{13}C$ values (Table 1), what processes might account for partial to full replacement of the test walls? Calcite etching implies a reduction in pH, consistent with precipitation from Fe-laden waters. In modern acid mine drainage environments, death of *Euglena mutablis*, a unicellular flagellate protist, results in authigenic precipitation of Fe minerals as the cell degrades (Brake et al., 2002). Over sufficient timescales these build up agglutinated hematitic biofilms, biomats and eventually travertine-like deposits (España et al., 2007). Hematite is readily precipitated from Fe-rich fluids by a wide microbial consortium (Brown et al., 1998). Note that the scale of the tests in the Elatina Formation allows us to dismiss that the materials were *primarily* precipitated by prokaryotes. Modern examples such as *Euglena mutablis* are at least an order of magnitude smaller than the tests described herein (Cavalier-Smith and Chao, 2003).

These considerations suggest that changes in basin water pH likely occurred at Brachina Gorge, trending to acid conditions following deposition (**Fig. 7**). Rose and

Maloof (2010) mapped systematic facies changes across the Elatina-Nucaleena boundary in the Flinders Ranges, identifying half –graben in the northern part of the ranges. They argued that regional extensional faults, inherited from a Sturtian phase of rifting, remained active into the Marinoan. This setting provides a suitable origin for ferriferous fluids, which may have been liberated along fault surfaces, providing a source of hematite.

Dalton et al. (2013) described a strikingly similar assemblage of agglutinated tests and tubes from carbonate laminites of the Rasthof Formation in northern Namibia- a post-Sturtian cap carbonate. In Brachina Gorge, a foraminiferal origin might potentially account for the whorl structures observed, the dimensions of the structures, and the range of forms. In this explanation, the sub-spherical forms might correspond to a well preserved (complete) test, and the non-spherical forms to cleaved or broken tests. Some modern unicellular eukaryotes, including foraminifera, bind mineral grains into their organic structure (agglutinates: Bosak et al., 2011 and refs therein), whereas others may biomineralise. The heterogeneous, spotty texture of the tests would tend to support the former mechanism.

Discussion

The occurrence of eukaryote tests within glaciogenic deposits of the Elatina Formation indicates that either 1) fossil material survived transport by Marinoan ice sheets during the second of two snowball Earth episodes (Hoffman and Schrag, 2002) or 2) the fossils accumulated on the tidally modulated braidplain, swept in on the rising tide. This latter origin is favoured on textural grounds. Sand and silt grains that

suffer subglacial or englacial transport exhibit characteristic surface microtextures. These include a tendency to be angular and facetted, with striae and conchoidal fractures (Immonen, 2013 and refs therein). In contrast, thin section and SEM analysis reveals grains that are rounded, with smooth surface textures. These characteristics are more typical of non-glacial to paraglacial contexts, to be expected in the forefield of an ice sheet beyond the grounding line where sediment reworking modifies surface microtextures.

Other Cryogenian eukaryote assemblages do not show close comparison to the material described herein. Chitinous, siliceous, or carbonate compositions are common (c.f. Bosak et al., 2012; Brain et al., 2012; Dalton et al., 2013), but the authors are unaware of any finds with a composite ferruginous-siliceous structure. It is notable that the depositional context for the Elatina fossil material also contrasts markedly with that of Cryogenian assemblages elsewhere. For example, the agglutinated eukaryotes described by Dalton et al. (2013) in Namibia represents the recovery of an ecosystem in the aftermath of the Sturtian glaciation (Bosak et al., 2012). In that example, the assemblage must reflect environmental amelioration, with thrombolite and stromatolite mounds charting the recovery of microbial carbonate factories in the same unit (Le Ber et al., 2015).

The precise origins of the eukaryote assemblage in the Elatina Formation remain ambiguous, and few meaningful comparisons can be made to strata containing agglutinated foraminifera, such as those in Namibia. They do, however, allow us to posit that either benthic or nektonic eukaryotes were able to thrive during the Marinoan glaciation, at least in South Australia. The occurrence of dropstone-bearing

diamictites immediately above and below the eukaryote-bearing sandstone bed at Brachina may point to an ecosystem that was active during the Marinoan glaciation. The presence of dropstones, testifying to ice rafting, implies either two pulses of glaciation or, more likely, the fluctuation of an ice margin on the sandur plain. In the latter case, it may be speculated that a eukaryote ecosystem, nourished by ferriferous waters from ongoing fault movement in the basin (Rose and Maloof, 2010), flourished during rather than after the demise of Marinoan ice masses.

Conclusions

- In Brachina Gorge, South Australia, the Elatina Formation comprises diamictites interbedded with sandstones and heterolithic deposits of unequivocal tidal origin. These deposits strongly support the notion of the presence of ice masses at or near sea level, and taken together with regional evidence from previous workers, point to a tidally modulated, glacially-influenced sandur for the upper part of the Elatina Formation;
- Though the diamictites are poorly exposed, deflected laminations beneath lonestones allow a waterlain origin to be deduced, for dropstones to be interpreted, and a case for direct glacial deposition to be proposed;
- A tidal sandstone bed, sandwiched above and below by diamictite, yields macroscopic, sand-sized hematite-silica agglutinates. Sub-circular forms, elongate to half-moon forms, and lozenge-shapes are all recognised. These are interpreted as fossil eukaryotes;
- The composition of the eukaryote tests is highly unusual, and comparable assemblages have not yet been found in equivalent strata on other continents. It is possible that Fe was sourced from fault zones in a regional extensional

basin context (Rose and Maloof, 2010). Nevertheless, organic carbon values of -20‰ $\delta^{13}C$ is consistent with a biogenic origin;

- The sedimentological context of the eukaryote test assemblage at Brachina Gorge raises the possibility of a thriving ecosystem during the Marinoan glaciation.

Acknowledgments. The authors are very grateful to both Sharon Gibbons for help with sample preparation and to Lauren Howard (formerly Natural History Museum, London) for undertaking the Nano-CT analyses for us. We benefitted from useful discussions with Joe Kirschvink, Tony Prave, Martin Kennedy and Kath Grey., and very helpful reviews from Breandán Anraoi MacGabhann, Catherine Rose, and anonymous colleagues. We would like to thank the editor, Philip Hughes, for his patience with us as we revised the manuscript.

References

BHATTACHARYYA, D.P., & KAKIMOTO, P.K. 1982. Origin of Ferriferous Ooids: An SEM Study of Ironstone Ooids and Bauxite Pisoids. *Journal of Sedimentary Petrology*, **52**, 849-857.

BOSAK, T., LAHR, D.J.G., PRUSS, S.B., MACDONALD, F.A., DALTON, L. & MATYS, E.D. 2011. Agglutinated tests in post-Sturtian cap carbonates of Namibia and Mongolia. *Earth and Planetary Science Letters*, **308**, 28–40.

BOSAK, T., LAHR, J.G., PRUSS, S.B., MACDONALD, F.A., GOODAY, A.J., DALTON, L., & MATYS, E.D. 2012. Possible early foraminiferans in post-Sturtian (713–636 Ma) cap carbonates. *Geology*, **40**, 67–70.

BRAIN, C.K., PRAVE, A.R., HOFFMANN, K-H., FALLICK, A.E., BOTHA, A., HERD, D.A., STURROCK, C., YOUNG, I., CONDON, D.J., & ALLISON, S.G. 2012. The first animals: ca. 760-million-year-old sponge-like fossils from Namibia. *South African Journal of Science*, **108**, Art. #658, 8 pages.

BRAKE, S.S., HASIOTIS, S.T., DANNELLY, H.K. & CONNORS, K.A. 2002. Eukaryotic stromatolite builders in acid mine drainage: Implications for Precambrian iron formations and oxygenation of the atmosphere? *Geology*, **30**, 599-602.

BROWN, D.A., SAWICKI, J.A. & SHERRIFF, B.L. 1998. Alteration of microbially precipitated iron oxides and hydroxides. *American Mineralogist*, **83**, 1419-1425.

CAVALIER-SMITH, T. CHAO, E. E.-Y. 2003. Phylogeny and Classification of Phylum Cercozoa (Protozoa). *Protist* **154** (3–4), 341–58.

DALTON, L.A., BOSAK, T., MACDONALD, F.A., LAHR, D.J.G., & PRUSS, S.B. 2013. Preservational and morphological variability of assemblages of agglutinated eukaryotes in Cryogenian cap carbonates of northern Namibia. *Palaios*, **28**, 67-79.

DAVIS, R.A. & DALRYMPLE, R.W. 2011. Principles of Tidal Sedimentology. Springer, 621pp.

ERICSSON, K.A. & SIMPSON, E. 2011. Precambrian Tidal Facies. *In*: DAVIS, R.A. & DALRYMPLE, R.W. (eds) *Principles of Tidal Sedimentology*, Springer, 397-419.

ESPAÑA, J-S., PASTOR, E.S., & LÓPEZ PAMO, E. 2007. Iron terraces in acid mine drainage systems: a discussion about the organic and inorganic factors involved in their formation through observations from the Tintillo acidic river (Riotinto mine, Huelva, Spain). *Geosphere*, **3**, 133-151.

EWING, R.C., EISENMAN, I., LAMB, M.P., POPPICK, L., MALOOF, A.C., & FISCHER, W.W. 2014. New constraints on equatorial temperatures during a Late Neoproterozoic snowball Earth glaciation. *Earth & Planetary Science Letters*, **406**, 110-122.

FAIRCHILD, I.J., FLEMING, E.J., BAO, H., BENN, D.I., BOOMER, I., DUBLYANSKY, Y.V., HALVERSON, G.P., HAMBREY, M.J., HENDY, C., MCMILLAN, E.A., SPÖTL, C., STEVENSON, C.T.E., WYNN, P.M. (in press). Continental carbonate facies of a Neoproterozoic panglaciation, NE Svalbard. *Sedimentology*. DOI: 10.1111/sed.12252

GRASSINEAU, N. 2006. High precision EA-IRMS analysis of S and C isotopes in geological materials. *Applied geochemistry*, **21**, 756-765.

HERBERT, C.M., ALEXANDER, J. & MARTÍNEZ DE ÁLVARO, M.J. 2015. Back-flow ripples in troughs downstream of unit bars: Formation, preservation and value for interpreting flow conditions. *Sedimentology*, DOI: 10.1111/sed.12203

HOFFMAN, P.F. & HALVERSON, G.P. 2008. Otavi Group of the western Northern Platform, the eastern Kaoko Zone and the western Northern Margin Zone. *In:* MILLER, R. MCG. (ed) *The Geology of Namibia. Volume 2- Neoproterozoic to Lower Palaeozoic*. Ministry of Mines and Energy, 13.69- 13-136.

HOFFMAN, P.F. & SCHRAG, D.P. 2002. The snowball Earth hypothesis: testing the limits of global change. *Terra Nova*, **14**, 129-155.

IMMONEN, N. 2013. Surface microtextures of ice-rafted quartz grains revealing glacial ice in the Cenozoic Arctic. *Palaeogeography, Palaeoclimatology, Palaeoecology*, **374**, 293-302.

IRELAND, T.R., FLÖTTMANN, T., FANNING, C.M., GIBSON, G.M. & PREISS, W.V. 1998. Development of the Early Paleozoic Pacific Margin of Gondwana from detrital zircon ages across the Delamerian Orogen. *Geology*, **26**, 243-246.

KENDALL, B., CREASER, R. A. & SELBY, D. 2006. Re–Os geochronology of postglacial black shales in Australia: Constraints on the timing of "Sturtian" glaciation. *Geology*, **34**, 729–732.

KNOLL, A.H., WALTER, M.R., NARBONNE, G.M. & CHRISTIE-BLICK, N. 2004. A New Period for the Geologic Time Scale. *Science*, **305**, 621-622.

KNOLL, A.H., JAVAUX, E.J., HEWITT, D. & COHEN, P. 2006. Eukaryotic organisms in Proterozoic oceans *Philos. Trans. R. Soc. Lond. B Biol. Sci*., **361**, 1023–1038

LE BER, E., LE HERON, D.P. & OXTOBY, N. 2015. Influence of microbial framework on Cryogenian microbial facies, Rasthof Formation, Namibia. *In*: BOSENCE, D. W. J., GIBBONS, K. A., LE HERON, D. P., MORGAN, W. A., PRITCHARD, T. & VINING, B. A. (eds) *Microbial Carbonates in Space and Time: Implications for Global Exploration and Production. Geological Society, London, Special Publications*, 418, 111-122.

LE HERON, D.P. 2012. The Location and Styles of Ice-Free "Oases" during Neoproterozoic Glaciations with Evolutionary Implications. *Geosciences*, **2**, 90-108.

LE HERON, D.P., COX, G., TRUNDLEY, A., & COLLINS, A.S. 2011. Cryogenian (Sturt and Elatina) glacial records of South Australia. *Precambrian Research*, **186**, 147–168.

LOUGHBREED, M.S. & MANCUSO, J.J. 1973. Hematite Framboids in the Negaunee Iron Formation, Michigan: Evidence for Their Biogenic Origin. *Economic Geology*, **68**, 202-209.

MAHAN, K. H., WERNICKE, B. P. & JERCINOVIC, M. J. 2010. Th–U–total Pb geochronology of authigenic monazite in the Adelaide rift complex, South Australia, and implications for the age of the type Sturtian and Marinoan glacial deposits. *Earth and Planetary Science Letters*, **289**, 76-86.

MALOOF, A.C., ROSE, C.V., BEACH, R., SAMUELS, B.M., CALMET, C.C., ERWIN, D.H., POIRIER, G.R., YAO, N., & SIMONS, F.J. 2010. Possible animal-body fossils in pre-Marinoan limestones from South Australia. *Nature Geoscience*, **3**, 653 – 659.

MAWSON, D. 1949a. Sturt tillite of Mount Jacob and Mount Warren Hastings, north Flinders Ranges. Transactions of the Royal Society of South Australia, v. 72, p. 244–251.

MAWSON, D. 1949b. The Elatina glaciation. A third occurrence of glaciation evidenced in the Adelaide System. *Transactions of the Royal Society of South Australia*, **73**, 117–121.

MAWSON, D. & SPRIGG, R.C. 1950. Subdivision of the Adelaide System. *Australian Journal of Science*, **13**, 69-72.

PRASHNOWSKY, A.A. 1999. Alfred Treibs memorial volume: dedicated to the memory of Alfred Treibs, the father of organic geochemistry, on the 100th anniversary of his birthday. *Halbig Durck, Munich*, 631p.

PREISS, W. 2005. Global stratotype for the Ediacaran System and Period- the Golden Spike has been placed in South Australia. *MESA Journal*, **37**, 20-25.

RAUB, T.D., EVANS, D.A.D. & SMIRNOV, A.V. 2007. Siliciclastic prelude to Elatina–Nuccaleena deglaciation: lithostratigraphy and rock magnetism of the base of the Ediacaran system. *In:* VICKERS-RICH, P. & KOMAROWER, P. (eds), *The Rise and Fall of the Ediacaran Biota*. Geological Society, London, Special Publications, **286**, 53-76.

REIDMAN, L.A., PORTER, S.M., HALVERSON, G.P., HURTGEN, M.T. & JUNIUM, C.K. 2014. Organic-walled microfossil assemblages from glacial and interglacial Neoproterozoic units of Australia and Svalbard. *Geology*, **42**, 1011-1014.

ROSE, C.V. & MALOOF, A.C. 2010. Testing models for post-glacial 'cap dolostone' deposition: Nuccaleena Formation, South Australia. *Earth and Planetary Science Letters*, **296**, 165-180.

ROSE, C.V., MALOOF, A.C., SCHOENE, B., EWING, R.C., LINNEMANN, U., HOFMANN, M., COTTLE, J.M. & BUDNICK, A. 2013. The end-Cryogenian glaciation of South Australia, Geoscience Canada (Hoffman Series), **40**, 256-293.

SCHMIDT, P.W. & WILLIAMS, G.E. 1995. The Neoproterozoic climatic paradox: equatorial palaeolatitude for Marinoan glaciation near sea level in South Australia. *Earth and Planetary Science Letters*, **134**, 107–124.

SHIELDS-ZHOU, G., HILL, A.C. & MACGABHANN, B.A. 2012. Chapter 17: The Cryogenian Period. *In*: GRADSTEIN, F.M., OGG, J.A., SCHMITZ, M. & OGG, G. (eds), *The Geological Time Scale 2012*, Elsevier B.V. pp394-411.

SOHL, L.E., CHRISTIE-BLICK, N., & KENT, D.V. 1999. Paleomagnetic polarity reversals in Marinoan (ca. 600 Ma) glacial deposits of Australia: implications for the duration of low-latitude glaciation in Neoproterozoic time. *Geological Society of America Bulletin*, **111**, 1120–1139.

VIDAL, G., & KNOLL, A. H. 1982, Radiations and extinctions of plankton in the late Proterozoic and early Cambrian. *Nature* , **297**, 57–60.

WILLIAMS, G.E., GOSTIN, V.A., MCKIRDY, D.M., & PREISS, W.V. 2008. The Elatina glaciation, late Cryogenian (Marinoan Epoch), South Australia: sedimentary facies and palaeoenvironments. *Precambrian Research*, **163**, 307–331.

Figure captions

Figure 1: Location of the study site in Brachina Gorge, and geological sketch map of the Adelaide Fold Belt in South Australia. Base map modified after Rose et al. (2013).

Figure 2: Stratigraphic context of the Elatina Formation within the central Flinders Ranges, showing global and regional chronostratigraphic subdivisions alongside lithostratigraphy. The Elatina Formation was deposited during the second (Marinoan) Neoproterozoic glaciation to affect the region. Stratigraphic column modified from Preiss et al. (1998).

Figure 3: Sedimentary log of the succession logged in Brachina Gorge in the topmost 22.5 m of the Elatina Formation. The stratigraphic position of each of the facies photographs shown in Fig. 4 is shown, together with the position of the bed sampled for microfossil material described in this paper. Location of measured section: 31°20.316'S 138°37.871'E. Section can be found along the Brachina Gorge geological trail and is approximately 100 m south of a sign pointing to the Elatina Formation ("Tillite").

Figure 4: Sedimentology of the Elatina Formation exposed at Brachina Gorge. A and A': heterolithic deposits interpreted as flaser beds. Note the presence of clay drapes on sigmoidal cross-lamina foresets, flame structures in mudstone intervals, and scour-and-fill structures on the cm-scale. B and B': Coset of climbing ripples above a scour-and-fill dominated sandstone interval. C and C': Contact between

lonestone-bearing, poorly stratified diamictite and cross-strata. D and D': Sedimentary features in the bed sampled for fossil material in this paper. Note the presence of wave-ripple geometries and counter-current ripples on the lower part of cross-bed foresets.

Figure 5: Thin section, SEM, and Nano-CT images of fossiliferous material. A and B: Thin section photomicrographs, in cross-polarised light, showing sub-circular, lozenge-shaped and half-moon shaped opaque fossils in a calcite-cemented siltstone. C and D: SEM images highlighting a whorl-shaped structure, and lozenge-shaped fossil. Each is characterized by an spotty texture. Note the rounded texture of neighbouring quartz grains. E: slice through a subsample of material imaged by Nano-CT, showing the predominance of half-moon structures interpreted as broken eukaryote tests. F, also a Nano-CT scan, shows these structures in more detail. G: Reference SEM image of an area of material subject to elemental mapping. H: Iron elemental map of the same area, demonstrating the elevated Fe in the fossil material. I: Silicon map, clearly identifying the quartz grains but also illustrating silica enrichment in the fossil material.

Figure 6; Selection of SEM images allowing the size and shape of the fossil material to be appraised, together with their relationship with the host sandstone. A: General view showing examples of semi-circular forms and lozenge shapes (to the left of the image). B: General view showing point contacts between grains and variable amounts of calcite core development within the fossils. C: Expanded view of the image shown on Fig. 5 C, with a well-developed whorl structure that is conjoined with linked lozenges. D: Magnified view of the conjoined lozenge to the left of the whorl shown in C. E: Continuous, >2 mm long, ribbon-like chains

of lozenges running down the middle of the image- these are compositionally and texturally identical to the sub-circular forms in ther upper part of the image. F: Magnified view of the upper left part of image E. G: A thin Fe and Si veneer around an etched calcite core. H: Further examples of Fe and Si veneers developed around an etched calcite core.

Figure 7: Taphonomic model as envisaged in a series of four sequential cartoons. A: Deposition of the carbonate tests on the sandy sea floor in alkaline, carbonate rich waters. B: Change in pore water chemistry (and potentially basin water chemistry) tending toward a lower pH, and the initial stages of etching of the calcite cores, accompanied by hematite replacement. C: Latter stages of etching with continued hematite replacement. D: A change in basin chemistry once again takes place during diagenesis, whereby calcite rhomb precipitation is facilitated to produce an equant spar.

Table 1: Carbon stable isotope data from ferruginous fossils in the Elatina Formation. Isotopic results are expressed in $\delta^{13}C_{V\text{-}PDB}$. The final two columns to the right are the mean values of the two analyses.

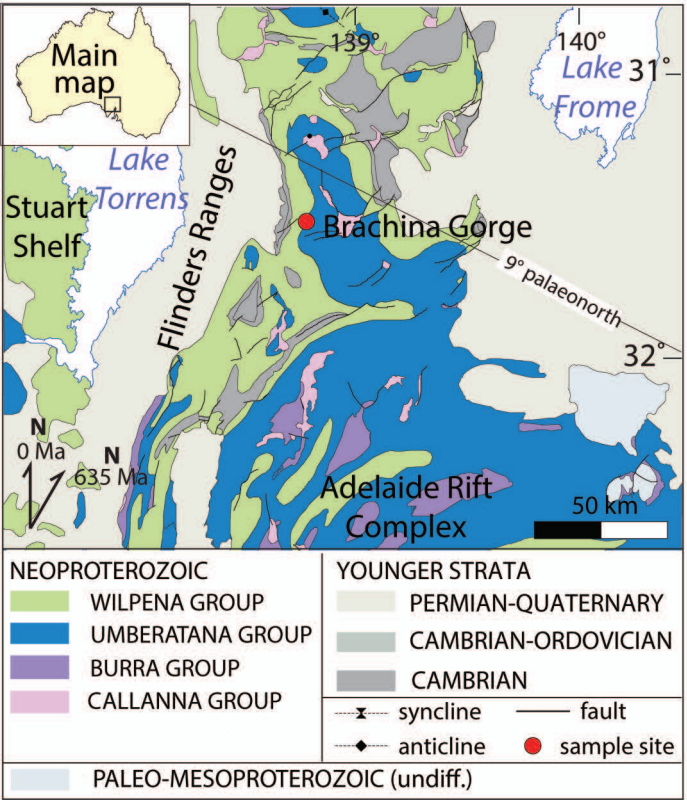
Main map
139°
140°
Lake Frome
31°
Lake Torrens
Stuart Shelf
Flinders Ranges
Brachina Gorge
9° palaeonorth
32°
N
0 Ma
N
635 Ma
Adelaide Rift Complex
50 km
NEOPROTEROZOIC
WILPENA GROUP
UMBERATANA GROUP
BURRA GROUP
CALLANNA GROUP
YOUNGER STRATA
PERMIAN-QUATERNARY
CAMBRIAN-ORDOVICIAN
CAMBRIAN
syncline
fault
anticline
sample site
PALEO-MESOPROTEROZOIC (undiff.)

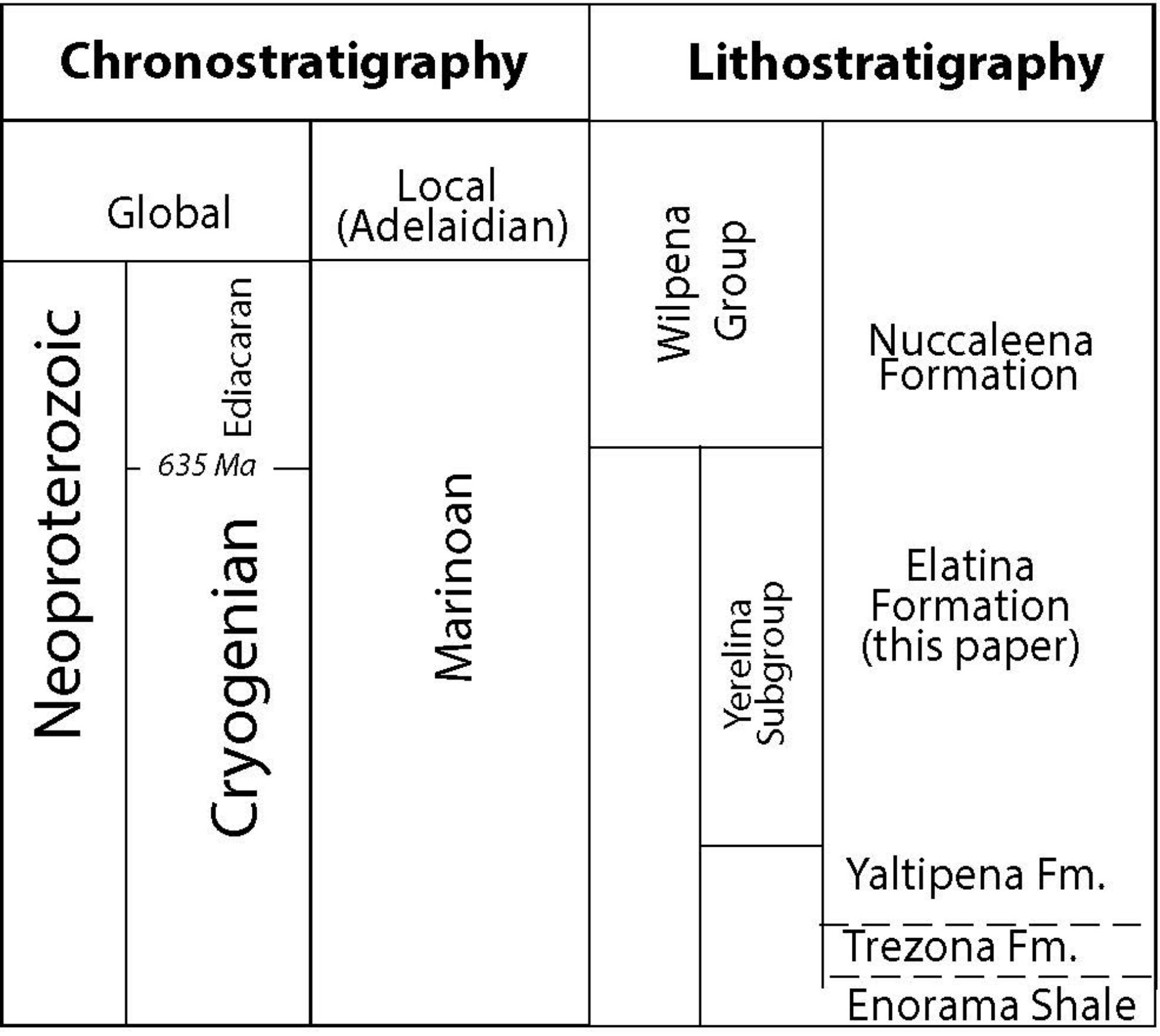
Chronostratigraphy
Lithostratigraphy
Global
Local (Adelaidian)
Neoproterozoic
Ediacaran
Cryogenian
635 Ma
Marinoan
Wilpena Group
Nuccaleena Formation
Yerelina Subgroup
Elatina Formation (this paper)
Yaltipena Fm.
Trezona Fm.
Enorama Shale

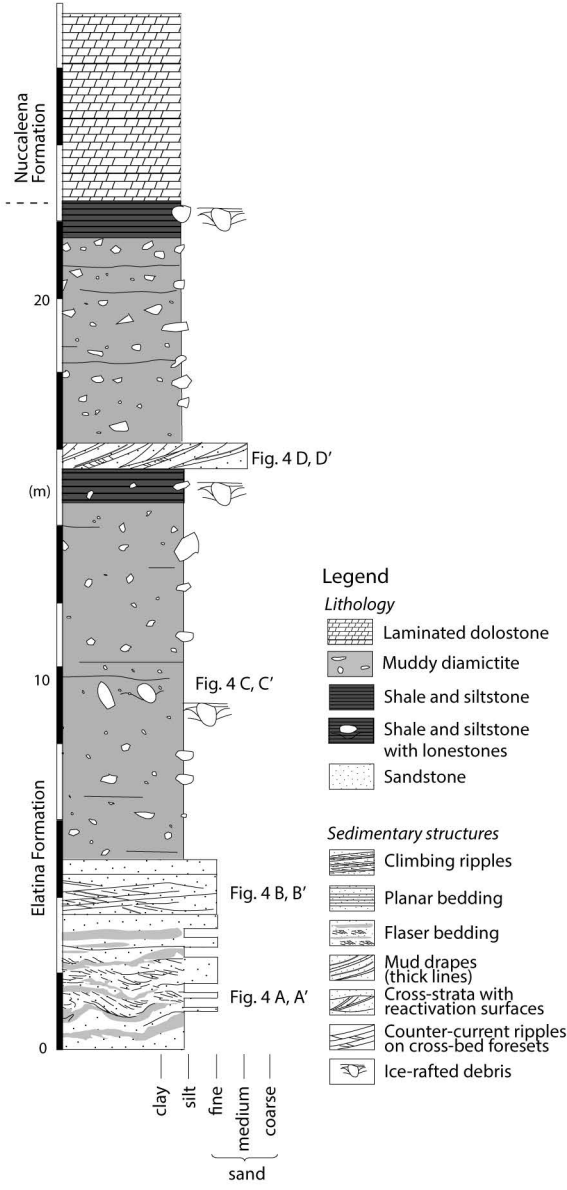
Nuccaleena Formation
20
(m)
10
0
Elatina Formation
Fig. 4 D, D′
Fig. 4 C, C′
Fig. 4 B, B′
Fig. 4 A, A′
clay
silt
fine
medium
coarse
sand
Legend
Lithology
Laminated dolostone
Muddy diamictite
Shale and siltstone
Shale and siltstone with lonestones
Sandstone
Sedimentary structures
Climbing ripples
Planar bedding
Flaser bedding
Mud drapes (thick lines)
Cross-strata with reactivation surfaces
Counter-current ripples on cross-bed foresets
Ice-rafted debris

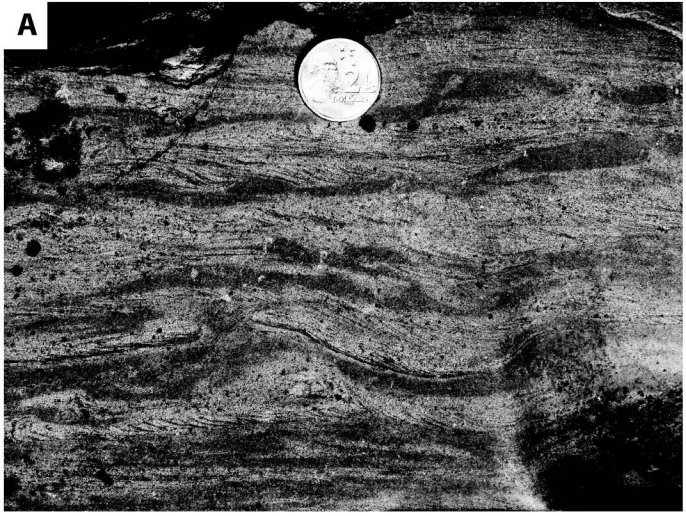
A

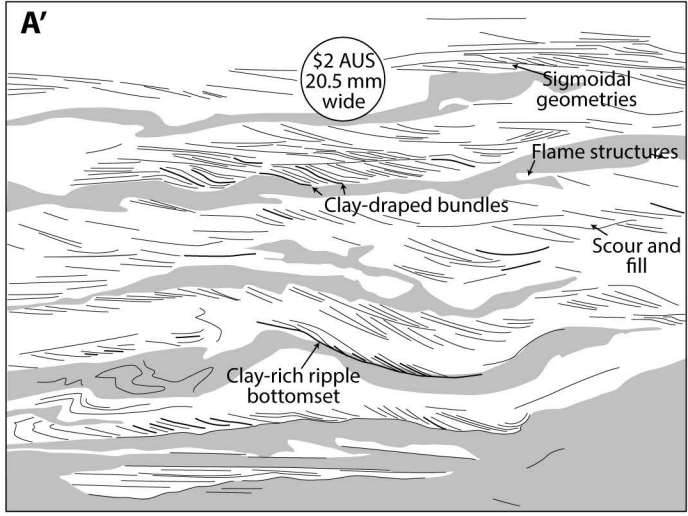
A′
$2 AUS
20.5 mm
wide
Sigmoidal
geometries
Flame structures
Clay-draped bundles
Scour and
fill
Clay-rich ripple
bottomset


B

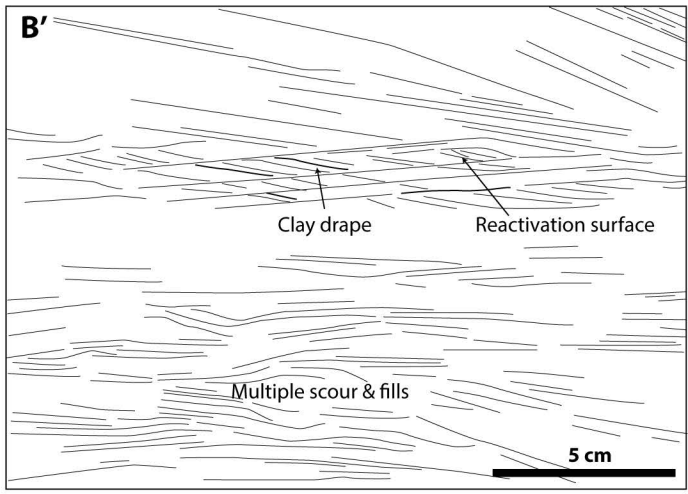
B′
Clay drape
Reactivation surface
Multiple scour & fills
5 cm


C

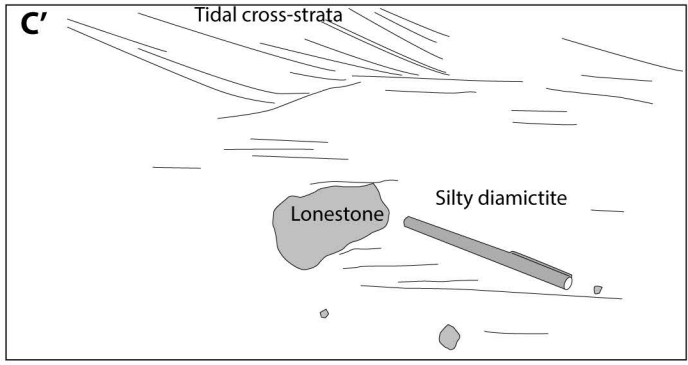
C′
Tidal cross-strata
Lonestone
Silty diamictite


D

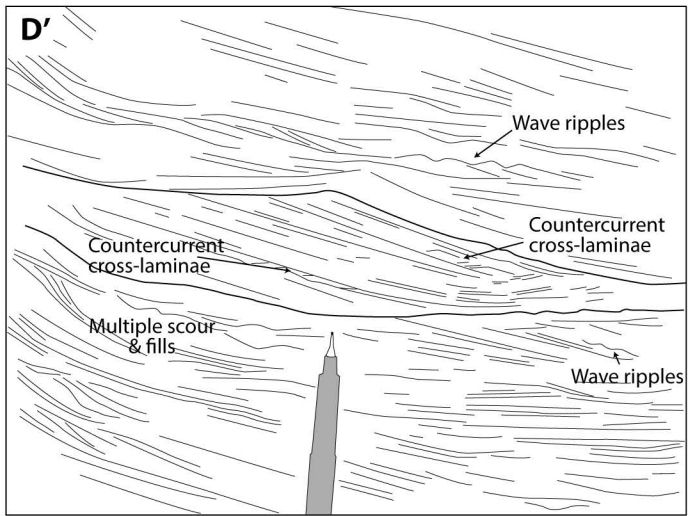
D′
Wave ripples
Countercurrent
cross-laminae
Countercurrent
cross-laminae
Multiple scour
& fills
Wave ripples

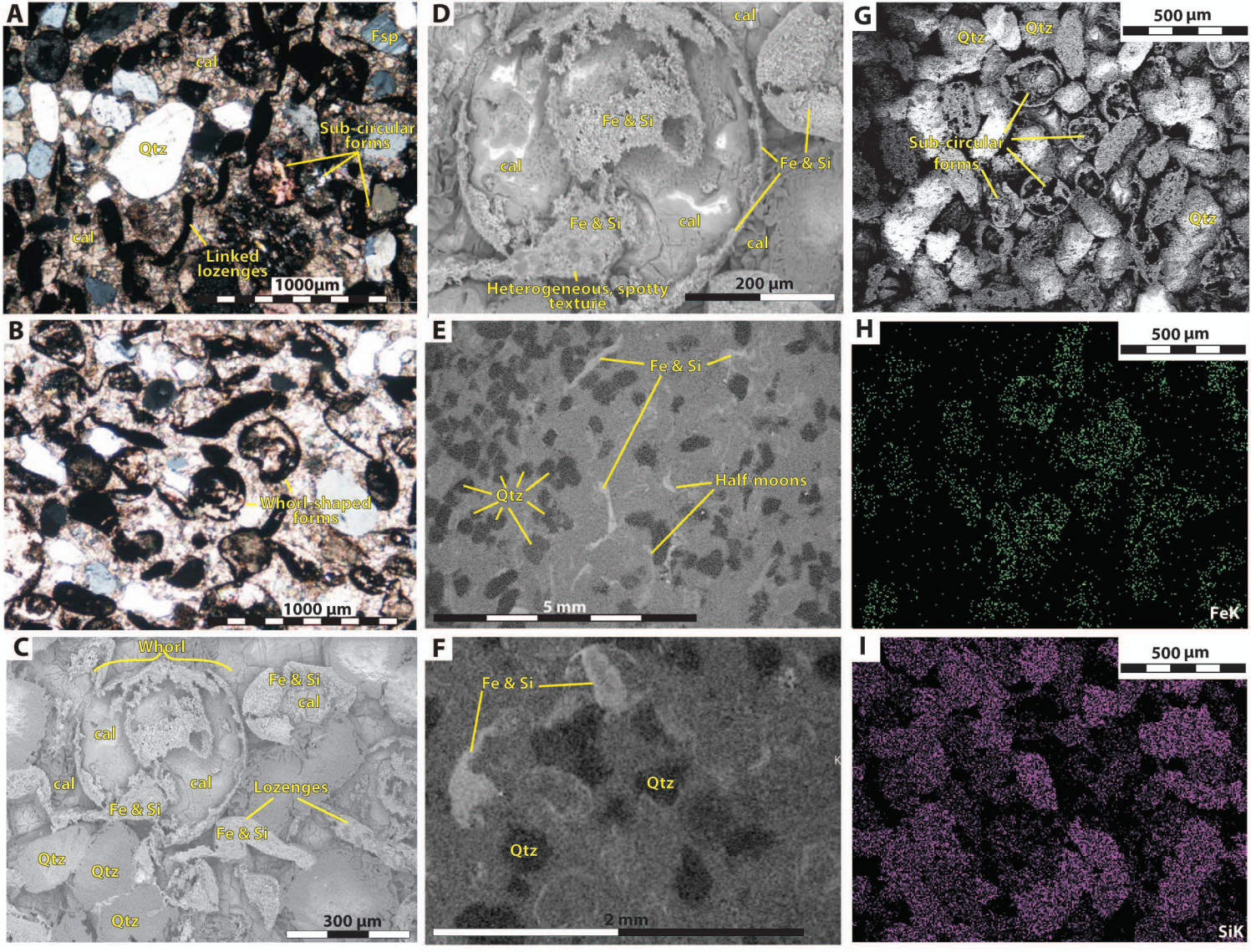
A
Fsp
cal
Qtz
Sub-circular forms
cal
Linked lozenges
1000µm
B
Whorl-shaped forms
1000 µm
C
Whorl
Fe & Si
cal
cal
cal
cal
Lozenges
Fe & Si
Fe & Si
Qtz
Qtz
Qtz
300 µm
D
cal
Fe & Si
cal
Fe & Si
Fe & Si
cal
cal
Heterogeneous, spotty texture
200 µm
E
Fe & Si
Qtz
Half-moons
5 mm
F
Fe & Si
Qtz
Qtz
2 mm
G
500 µm
Qtz
Qtz
Sub-circular forms
Qtz
H
500 µm
FeK
I
500 µm
SiK

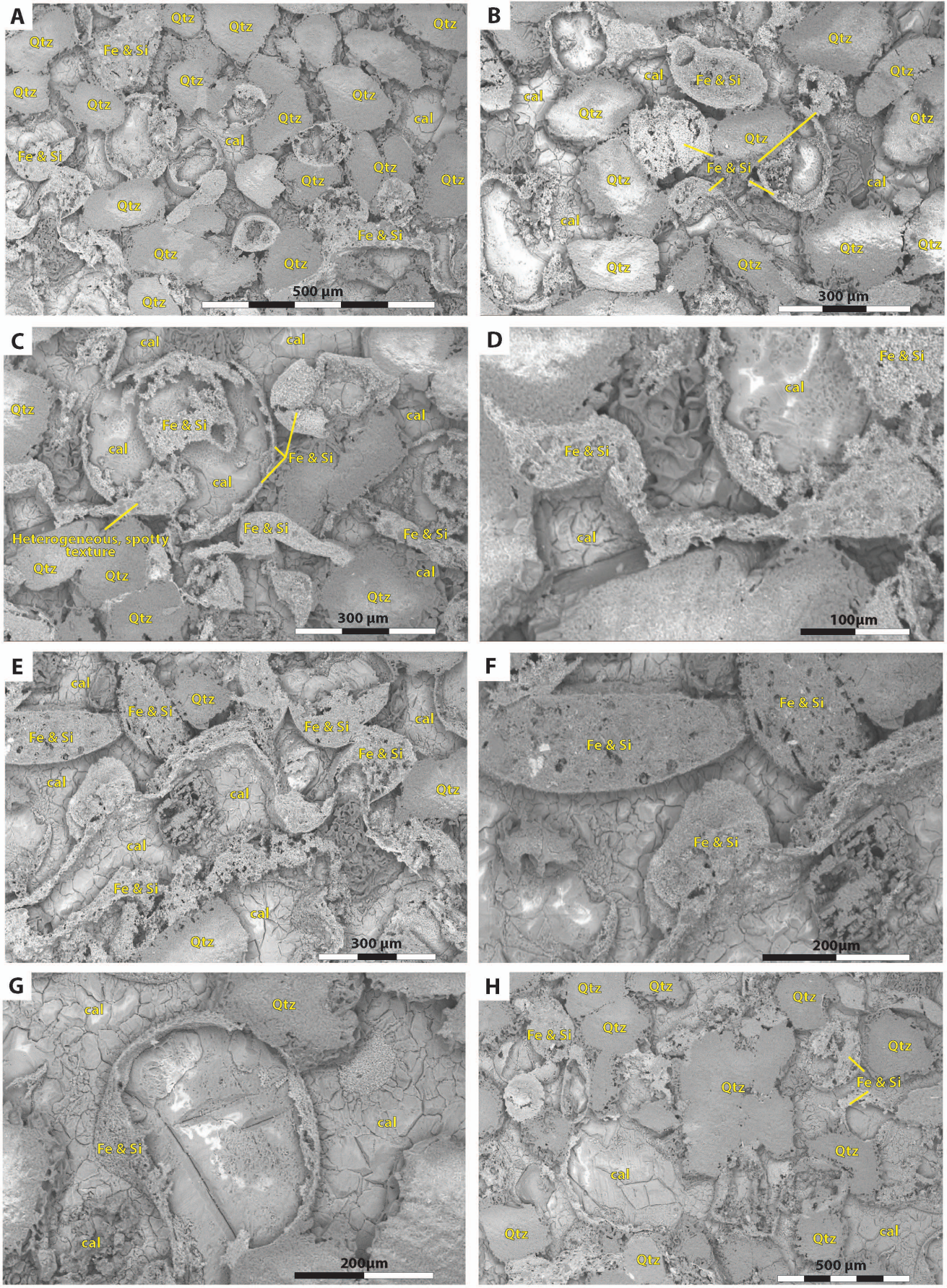
A
Qtz
Fe & Si
cal
500 µm
B
300 µm
C
Heterogeneous, spotty texture
300 µm
D
100µm
E
300 µm
F
200µm
G
200µm
H
500 µm

Figure 6

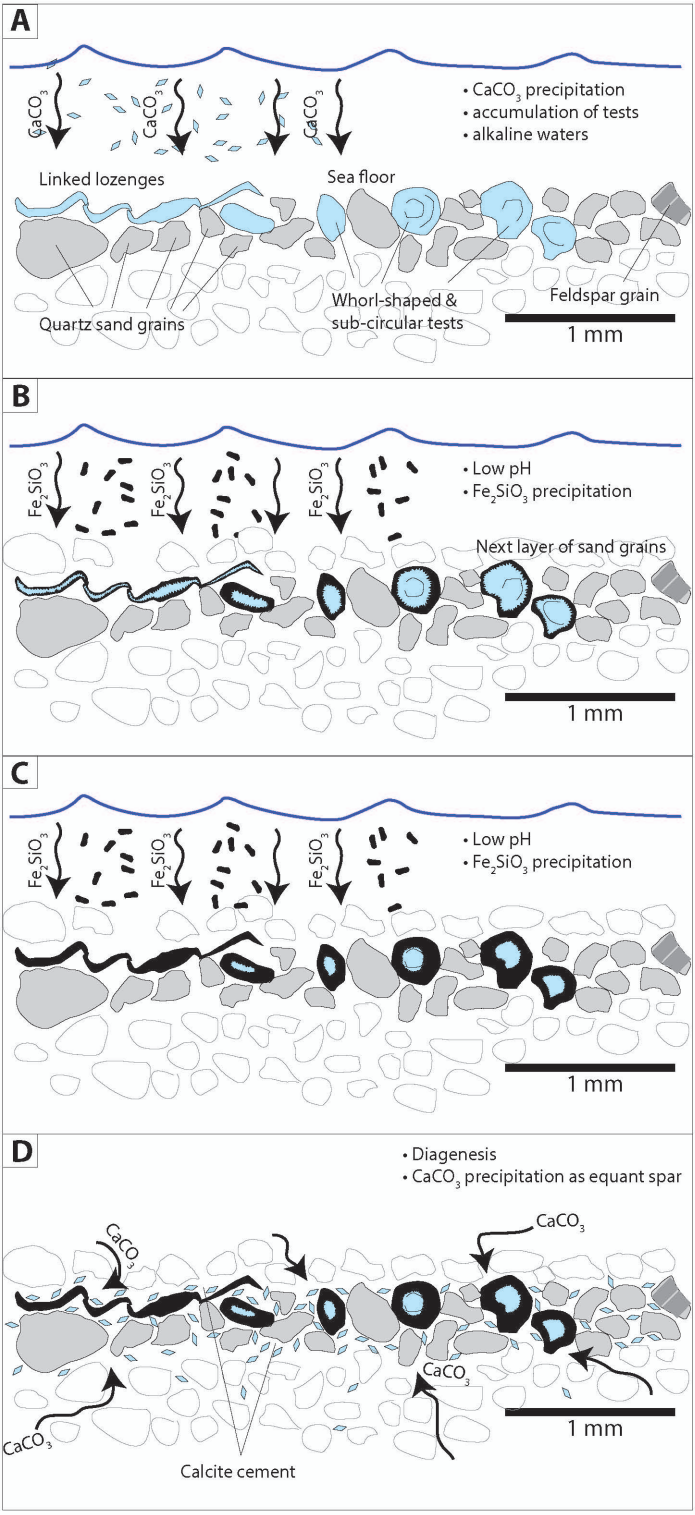
A
CaCO3
CaCO3
CaCO3
• CaCO3 precipitation
• accumulation of tests
• alkaline waters
Linked lozenges
Sea floor
Quartz sand grains
Whorl-shaped &
sub-circular tests
Feldspar grain
1 mm
B
Fe2SiO3
Fe2SiO3
Fe2SiO3
• Low pH
• Fe2SiO3 precipitation
Next layer of sand grains
1 mm
C
Fe2SiO3
Fe2SiO3
Fe2SiO3
• Low pH
• Fe2SiO3 precipitation
1 mm
D
• Diagenesis
• CaCO3 precipitation as equant spar
CaCO3
CaCO3
CaCO3
CaCO3
1 mm
Calcite cement

Figure 7